Accepted with major revisions in IEEE Trans. Antennas and Propagation, 2024

A HIE S-FDTD method to account for geometrical and material uncertainties in lossy thin panels

Miguel R. Cabello, Luis D. Angulo, Alberto Gascón, Salvador G. Garcia, Alberto Prados, Guadalupe G. Gutierrez, Enrique Pascual-Gil, Miriam G. Atienza

***Abstract*—This paper introduces an extended Stochastic Finite-Difference Time-Domain (S-FDTD) method tailored to analyze thin panel structures. It aims to predict the standard deviation and probability density function (PDF) of electromagnetic magnitudes (fields and currents), assuming their uncertainties in geometrical and material parameters are both known. The method to account for the sub-cell nature of the thin panel method used is based on the broadly tested subgridding boundary condition (SGBC) approach. This method employs an implicit-explicit hybrid (HIE) scheme in an unconditional Crank-Nicolson (CN) formulation (CN-SGBC), ensuring that it does not introduce any extra limitations to the standard stability criterion of the FDTD method. In the article, classical models of explicit formulations of S-FDTD are extended to the FD-CNTD HIE formulation.**

***Index Terms*—FDTD, Montecarlo, stochastic methods, lossy thin panel modeling**

I. Introduction

THE finite difference time domain (FDTD) method [1] is probably the most widely used one in electromagnetic analysis. It replaces the space and time derivatives in Maxwell curl equations with second-order accurate finite differences [2] to find a method capable of finding the wideband response of complex systems, including their whole material and geometrical complexity.

Modern materials in aeronautical and automotive industries often consist of multilayered carbon-fiber composite (CFC) thin panels with lower electrical conductivity than most metals. FDTD cannot simulate these thin structures in a computer-affordable manner because they require tiny mesh sizes to resolve their thickness and skin depth correctly. Instead, equivalent sub-cell models are employed, like the classical network impedance boundary conditions (NIBC) method [3], [4]. NIBC assumes a 1D wave propagation along the thin panel thickness to find the fields at its outer faces in a convolutional manner, thanks to the quasi-TEM nature of fields propagating into the lossy slab after refraction for whatever incidence [5].

Late-time instabilities reported for the NIBC method led the authors to present an alternative approach based on the SGBC in [5] also used in [6]. SGBC, instead, uses an explicit wave propagator to find the fields at the thin panel's outer faces by using a 1D fine mesh inside it. A convenient FDTD scheme to find the fields inside the thin panel is the unconditionally stable 1D Crank-Nicolson time-domain (CNTD) method. It can be hybridized naturally to the usual 3D Yee-FDTD, kept for the more coarsely meshed 3D region, by utilizing a hybrid implicit-explicit (HIE) algorithm. The unconditional stability of the resulting scheme safeguards the computer affordability of the whole algorithm by using the same time-step both inside and outside it, at the small cost of requiring the solution of a tridiagonal implicit algorithm at each time step only inside the thin panel.

The so-called stochastic FDTD methods [7] are an extension of FDTD to predict uncertainties in the fields due to material uncertainties. These are becoming a powerful alternative to replace the costly multidimensional parameter-sweeping typical approaches, usually resorting to brute-force Montecarlo (MC) random simulations. S-FDTD simultaneously finds the expected value and standard deviation on the fields as a function of those of the material constitutive parameters, roughly with twice the time of a single FDTD run. In [8], we have been extended to the thin wire sub-cell Holland's technique [9], giving a simple implementation in existing FDTD codes, assuming they are already programmed with the usual message passing interface (MPI) parallel paradigm. Most S-FDTD works put forth the argument that a single S-FDTD simulation can provide reasonable predictions for MC-FDTD results under the assumption of a unity correlation between material properties across spatial points and a probability density function (PDF) with a small standard deviation for the material uncertainties. In [8], the authors showed that the standard deviation for media (non-correlated) could also be determined by performing one S-FDTD simulation per each material with non-null standard deviation and combining the results, which is less computationally intense than a brute-force MC approach.

FDTD method was also extended to include the measurement of geometric uncertainties in fields and currents, referred to as the geometrical S-FDTD (GS-FDTD). The concept of GS-FDTD was first introduced in [10]. In a subsequent study [11], a method was proposed that accounted for both geometry and media uncertainties. However, it is essential to note that both works only addressed problems in one or two dimensions.

In this paper, we extend the classical explicit formulation of S-FDTD from [7], [11], and [8] to an HIE formulation, allowing us to predict the impact on the electromagnetic

The work described in this paper have been supported by the Spanish MCIN and EU FEDER I+D+i project PID2019-106120RB-C33. PID2022-137495OB-C31, by the Junta de Andalucia FEDER project B-TIC-700-UGR20, and by the ICARO project funded by the UGR grant 241504 in 2020

The first four authors are with the Dept. of Electromagnetism, University of Granada (UGR), Fuentenueva s/n, 18071 Granada, Spain. Authors 5th-7th are with Airbus, P. John Lennon s/n, 28906 Getafe, Spain. A. Prados (now in Airbus DS) performed his work under contract for the UGR during 2022, and M. G. Atienza performed with work for the UGR under an ICARO grant in 2020. Corresponding author e-mail: mcabello@ugr.es

magnitudes of geometrical and material uncertainties of lossy thin panels. We utilize the CN-SGBC method proposed in [5] to achieve this.

It has been validated with analytical planar test cases and with a simple representative model of a composite fuselage, including some wiring inside. This situation is of critical importance for the aeronautical industry since the current coupled to cables connecting equipment on a modern aircraft poses a significant hazard in the context of Lightning Indirect Effects (LIE) assessment.

II. CN-SGBC FUNDAMENTALS

CN-SGBC (as NIBC) starts by assuming that waves inside a lossy thin panel propagate perpendicularly to its faces, regardless of the actual angle of incidence and thin panel thickness. This assumption proved [5] to be a good approximation for most lossy materials of aeronautical interest in their typical frequencies of interest. CN-SGBC employs a 1D CN-FDTD wave propagator inside the thin panel to find the tangential E-fields at each face. Its thickness d is meshed into N fine cells, with a $\Delta_{\text{fine}} = \mathrm{d}/N$, accordingly chosen to the wavelength and skin depth at the maximum frequency. CN-SGBC combines the 1D scheme with the usual 3D one outside the thin panel see fig. 1, for which a coarse grid of size Δ_{coarse}, typically much larger than Δ_{fine}, is taken using the classical space resolution criterion [2].

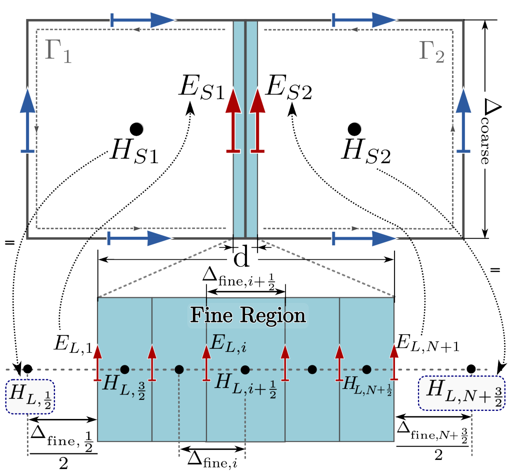

Fig. 1. Cross section of an FDTD cell with an SGBC boundary.

The main difference between CN-FDTD and the classical Yee-FDTD is that the E- and H-field components are co-located in time (e.g., at an integer multiple of the time step). In contrast, the space locations are the staggered integer and semi-integer Yee typical ones. We can summarize the algorithm as follows. Let us assume that the thin panel is homogeneous with constant permittivity ε, permeability μ, and electric conductivity σ_e (see also [12] for a dispersive formulation), and let us denote the electric and magnetic 1D field components inside the thin panel by E_i and H_i. A tridiagonal system of equations is solved at each time step by a back-substitution inversion algorithm to find the E_i field components inside the thin panel (for $i = 0, \ldots, N+1$)

$$\begin{aligned} bE_1^{n+1} + cE_2^{n+1} &= d_1^n \\ aE_{i-1}^{n+1} + bE_i^{n+1} + cE_{i+1}^{n+1} &= d_i^n \\ aE_N^{n+1} + bE_{N+1}^{n+1} &= d_{N+1}^n \end{aligned} \tag{1}$$

and, the magnetic field components (for $i = 1, \ldots, N$) are found from them in an explicit manner by

$$\begin{aligned} H_{i+1/2}^{n+1} = {} & D_a H_{i+1/2}^n + \\ & \frac{D_b}{2}\left(E_i^n - E_{i+1}^n + E_i^{n+1} - E_{i+1}^{n+1}\right) \end{aligned} \tag{2}$$

with i, n denoting the space and time locations where the electric and magnetic fields are sampled in the fine region. The coefficients in (1) are:

$$a = \left(-\frac{C_b D_b}{4}\right), \; c = \left(-\frac{C_b D_b}{4}\right), \; b = (1 - a - c) \tag{3}$$

$$\begin{aligned} d_i^n = {} & \left(\frac{C_b}{2}\right)(1 + D_a)\left(H_{i-1/2}^n - H_{i+1/2}^n\right) \\ & + \left(\frac{C_b D_b}{4}\right)\left(E_{i-1}^n + E_{i+1}^n\right) + \left(C_a - \frac{C_b D_b}{2}\right) E_i^n \end{aligned} \tag{4}$$

with C_a, C_b, D_a, D_b functions of the thin panel properties:

$$\begin{aligned} C_a &= \frac{2\varepsilon - \Delta t \sigma_e}{2\varepsilon + \Delta t \sigma_e}, \; C_b = \frac{2\Delta t}{(2\varepsilon + \Delta t \sigma_e)\mathrm{d}/N} \\ D_a &= 1, \; D_b = \frac{\Delta t}{\mu \mathrm{d}/N} \end{aligned} \tag{5}$$

The HIE scheme, as described in [5], utilizes the magnetic fields H_{S1} and H_{S2} from the conventional Yee-scheme, where H_{S1} corresponds to $H_{L,3/2}$ and H_{S2} corresponds to $H_{L,N+3/2}$. The magnetic fields H_{S1} and H_{S2} are updated using the electric fields E_{S1} and E_{S2} respectively. Specifically, E_{S1} corresponds to E_1 and E_{S2} corresponds to E_{N+1}. The values of E_1 and E_{N+1} are determined by solving Equation (1).

The classical 3D Yee FDTD scheme finds the rest of E-H fields outside the thin panel. Both regions communicate naturally through these components, which play the role of external source terms for CNTD. As a result, the unconditional stability of the CNTD algorithm is preserved, and the same time-step can be used both inside and outside the thin panel.

III. S-FDTD FOR CN-SGBC EQUATIONS

The impact of the uncertainty of the material properties on their shielding effectiveness can be predicted by extending the S-FDTD method of [7] to the CN-SGBC equations, using the same methodology first introduced in [8] for thin wire Holland's equations.

The mean values of the fields are proven to be advanced by S-FDTD also with Eqs. (1)(2). Their standard deviation $\sigma\{\}$ is found[1] by using the Delta method, which states in general

$$\sigma^2\{f(x_1,...,x_N)\} \simeq \sum_{\forall i}\left(\left.\frac{\partial f}{\partial x_i}\right|_{\mu\{x_1\},...}\right)^2 \sigma^2\{x_i\}+ \sum_{\forall i,j,i\neq j} 2\left.\left(\frac{\partial f}{\partial x_j}\frac{\partial f}{\partial x_i}\right)\right|_{\mu\{x_1\},...} \sigma\{x_i\}\sigma\{x_j\}\rho_{x_i,x_j} \quad (6)$$

with ρ_{x_i,x_j} denoting the usual Pearson correlation coefficient and $\mu\{\}$ denote de mean value.

Applying the Delta method to all the additive and multiplicative terms in the CNTD scheme, we find a set of advancing equations for the fields inside and at the thin panel boundaries formally identical to (1) (2). The only difference is found in the addition of a set of independent sources, which in turn depend on the mean values previously found by Eqs. (1)(2), only at locations with some material uncertainty. Hence, the advancing equation for the deviation in the internal 1D E-field employs a tridiagonal system of equations, the counterpart of (1), but modified to take into account the non-null deviation in ε, σ_e,

$$\sigma\left\{aE_{i-1}^{n+1} + bE_i^{n+1} + cE_{i+1}^{n+1}\right\} = \sigma\{d_i^n\} \quad (7)$$

which leads, after some algebra, to

$$\begin{aligned} &a\sigma\left\{E_{i-1}^{n+1}\right\} + b\sigma\left\{E_i^{n+1}\right\} + c\sigma\left\{E_{i+1}^{n+1}\right\} = d_i^n|_{\text{C,D}}- \\ &-\sigma\{a\}E_{i-1}^{n+1} - \sigma\{b\}E_i^{n+1} - \sigma\{c\}E_{i+1}^{n+1} + d_i^n|_{\text{E,H}} \end{aligned} \quad (8)$$

with

$$\begin{aligned} d_i^n|_{\text{C,D}} = &\left(\frac{C_b}{2}\right)(1+D_a)\left(\sigma\left\{H_{i-1/2}^n\right\} - \sigma\left\{H_{i+1/2}^n\right\}\right) \\ &+\left(\frac{C_bD_b}{4}\right)\left(\sigma\left\{E_{i-1}^n\right\} + \sigma\left\{E_{i+1}^n\right\}\right) \\ &+\left(C_a - \frac{C_bD_b}{2}\right)\sigma\left\{E_i^n\right\} \end{aligned} \quad (9)$$

$$\begin{aligned} d_i^n|_{\text{E,H}} = &\,\sigma\left\{\left(\frac{C_b}{2}\right)(1+D_a)\right\}\left(H_{i-1/2}^n - H_{i+1/2}^n\right) \\ &+\sigma\left\{\left(\frac{C_bD_b}{4}\right)\right\}\left(E_{i-1}^n - E_{i+1}^n\right) \\ &+\sigma\left\{\left(C_a - \frac{C_bD_b}{2}\right)\right\}E_i^n \end{aligned} \quad (10)$$

The deviation in the H-field (assuming null deviation in the permeability $\sigma\{\mu\} = 0$ for simplicity) is found by the following equation, the counterpart of (2)

$$\begin{aligned} &\sigma\{H_{i+1/2}^{n+1}\} = \frac{D_a}{den}\sigma\{H_{i+1/2}^n\}+ \\ &\frac{D_b}{2}\left(\sigma\{E_i^n\} - \sigma\{E_{i+1}^n\} + \sigma\{E_i^{n+1}\} - \sigma\{E_{i+1}^{n+1}\}\right)+ \\ &\sigma\left\{\frac{D_b}{2}\right\}\left(E_i^n - E_{i+1}^n + E_i^{n+1} - E_{i+1}^{n+1}\right) \end{aligned} \quad (11)$$

[1]We will employ the usual notation of $\sigma\{u\}$ to denote the standard deviation of any variable u, not to be confused with the electric conductivity noted by σ_e.

The standard deviation in the updating constants in (8)(9)(10) and (11) are found formally using the usual chain rule for the derivative of a multi-variate function [8]. Just note that all the updating coefficients C_a, C_b, D_a, D_b are generic functions $u(\varepsilon, \sigma_e, \text{d})$. Hence, we can write

$$\sigma\{u(\varepsilon,\sigma_e,\text{d})\} \equiv \frac{\partial u}{\partial \varepsilon}\sigma\{\varepsilon\} + \frac{\partial u}{\partial \sigma_e}\sigma\{\sigma_e\} + \frac{\partial u}{\partial \text{d}}\sigma\{\text{d}\} \quad (12)$$

where Pearson cross-correlation coefficients have been assumed to be unity (see [8], [13] for a deeper discussion). The partial derivatives in (12) can be performed either analytically or numerically (e.g., by a second-order finite-centered formula).

The modifications on the rest of the HIE algorithm of [5], as well as the external Yee 3D FDTD scheme, are also performed following the same idea (the usual S-FDTD equations of [7] are yielded outside the thin panel).

Let us stress again that Eqs. (8)(11) are a counterpart of Eqs. (1)(2), respectively, just adding the mean values (of present and past fields) found by (1)(2) as *source* independent terms. Hence, the computer implementation of this method into an existing FDTD program is straightforward since S-FDTD only uses FDTD values as independent sources at each time step, thanks to the MPI paradigm described in [8], that can be extended here in an entirely similar fashion. This S-FDTD implementation typically multiplies by roughly a factor 2 both the memory and the CPU time. Hence, the computational savings become apparent, considering that typical MC populations require several thousands of simulations.

IV. Validation in a canonical problem

As a first proof-of-context, let us consider a canonical test case consisting of an indefinite panel with losses. The panel is illuminated with a normal plane wave and a sinusoidal profile with amplitude unit and frequency 1 Ghz. The panel has a constant conductivity of 10^3 S/m, the mean value of the thickness is 10^{-4} m and we assume that the thickness has an uncertainty with a Gaussian PDF. We evaluate the amplitude and its uncertainty of the transmitted electric field, using MC-FDTD, and S-FDTD, for two different uncertainties in panel thickness: $\sigma\{\text{d}\} = 0.1\,\mu\{\text{d}\}$ and $\sigma\{\text{d}\} = 0.25\,\mu\{\text{d}\}$. For the MC-FDTD and S-FDTD simulations, we have used a 3D-FDTD with a cubic grid of 5 mm and CFLN of 0.99. The panel is modeled using the thin panel technique based on the CN-SGBC method. The FDTD domain is truncated with proper boundary conditions: PMLs at the termination planes in the propagation direction and PEC/PMC in the E-H plane, according to the polarization, to preserve a TEM plane-wave propagation. The simulation results are compared in Table I with MC-theoretical used as a reference. The MC-theoretical are obtained using MC and the theoretical transmission coefficient with the usual analytical formula:

$$T = \frac{2\eta_0\eta\sinh(\gamma\text{d})}{\left(\eta_0\sinh(\gamma\text{d}) + \eta\cosh(\gamma\text{d})\right)^2 - \eta^2} \quad (13)$$

Fig 2 and Fig 3 depict the results obtained by assuming a relative standard deviation of thickness $\sigma\{\text{d}\} = 0.1\,\mu\{\text{d}\}$

TABLE I
MEAN AND STANDARD DEVIATION RESULTS OF THE AMPLITUDE FOR A GAUSSIAN PDF.

$\sigma\{\mathrm{d}\}$	$\mu\{\text{Amplitude}\}$; $\sigma\{\text{Amplitude}\}$		
	MC-Theoetical	MC-FDTD	S-FDTD
$0.1\,\mu\{\mathrm{d}\}$	0.0513; 0.0052	0.0519; 0.0052	0.0504; 0.0048
$0.25\,\mu\{\mathrm{d}\}$	0.0664; 0.0453	0.0667; 0.0423	0.0504; 0.0120

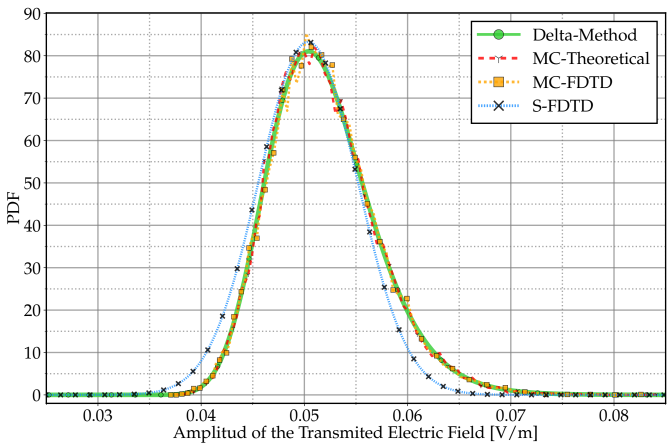

Fig. 2. PDF of the amplitude of the transmitted electric field at 1 GHz under normal incidence, through a panel with $\sigma_e = 1$ kS/m, and thickness of Gaussian distribution with $\mu\{\mathrm{d}\} = 0.1$ mm, $\sigma\{\mathrm{d}\} = 0.1\,\mu\{\mathrm{d}\}$

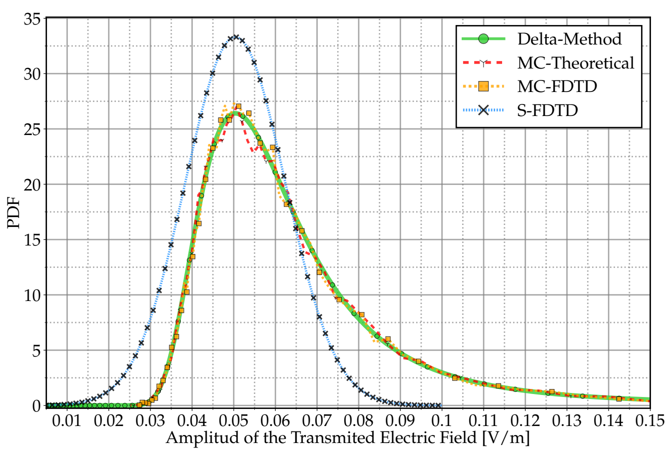

Fig. 3. PDF of the amplitude of the transmitted electric field at 1 GHz under normal incidence, through a panel with $\sigma_e = 1$ kS/m, and thickness of gaussian distribution with $\mu\{\mathrm{d}\} = 0.1$ mm, $\sigma\{\mathrm{d}\} = 0.25\,\mu\{\mathrm{d}\}$

and $\sigma\{\mathrm{d}\} = 0.25\,\mu\{\mathrm{d}\}$, respectively. Additionally, Table I presents the mean and standard deviation values for the amplitude based on a Gaussian PDF. From Fig.2, we notice, as expected, that the S-FDTD method does not preserve the Gaussian shape for the PDF assumed for the PDF of the independent variables, which becomes apparent in Fig 3 where the deviation of them if much larger than for Fig 2. The reason for this lies in the Delta method, which assumes a series truncated in the second-order terms

$$\begin{aligned}\mu\{\mathrm{g}(R)\} &= \mathrm{g}(\mu\{R\}) + \mathcal{O}\left[(R-\mu\{R\})^2\right],\\ \sigma\{\mathrm{g}(R)\} &= \mathrm{g}'(\mu\{R\})\,\sigma\{R\} + \mathcal{O}\left[(R-\mu\{R\})^2\right]\end{aligned} \tag{14}$$

where g represents a generic function. However, we can reasonably assume that the Gaussian distribution is preserved with a good approximation when the standard deviation is sufficiently small.

V. APPLICATION TO A REALISTIC PROBLEM

We finally illustrate the application of this method to a more complex case of aeronautical interest: a typical LIE assessment test case. To verify the ability to predict the variability of the induced current in wires due to intrinsic uncertainty of the CFC conductivity and thickness, we have studied the case in Fig. 4, which is a single-wire version of a test case used in [14]. It consists of a simplified scaled fuselage model with all the surfaces made of CFC panels and with a wire inside loaded with $50\,\Omega$ in both ends. For the LIE assessment, we used a direct current injection (DCI) source in the time domain with a waveform-A profile [15]. We denote this current as I_{DCI}, which is injected at one end of the simplified fuselage, and taken out by an exit point, consisting of a PEC line connected to the absorbing boundary conditions at the other end.

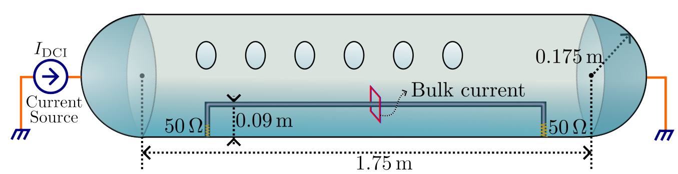

Fig. 4. Simplified fuselage model. The size of this object is 1.75m x 0.35 m x 0.35m. The wire inside is 1m long and is centered along the structure. It is situated at a height of 0.09 m over the cylinder and grounded through $50\,\Omega$ resistances to its lateral face at its ends [14].

For the simulation (MC-FDTD and S-FDTD), the model was meshed with a cubic grid with 10 mm of cell size. The wire is treated employing the usual Holland thin wire approximation [9] and the CFC using the CN-SGBC method. A CPU time of 240 minutes in an Intel Xeon 48-core node was required for each FDTD simulation[2].

In this test case, we evaluate the uncertainties in the intensity of the wire $\sigma\{I_{\mathrm{w}}\}$ due to the uncertainties in the thickness and conductivity of the CFC material. The values of CFC conductivity are assumed to have a mean value $\sigma_e = 1$ kS/m, and a standard deviation of $\sigma\{\sigma_e\} = 0.1\,\sigma_e$. For the CFC thickness, a mean value of $\mathrm{d} = 10^{-4}$ m and a standard deviation of $\sigma\{\mathrm{d}\} = 0.1 \cdot \mathrm{d}$ are used. The following expression combines the variability of both parameters

$$\sigma\{I_{\mathrm{w}}\} = \sqrt{\begin{array}{c}\sigma^2\{I\}\big|_{\substack{\sigma\{\mathrm{d}\}\neq 0,\\ \sigma\{\sigma_e\}=0}} + \sigma^2\{I\}\big|_{\substack{\sigma\{\mathrm{d}\}=0,\\ \sigma\{\sigma_e\}\neq 0}} + \\ +2\,\sigma\{I\}\big|_{\substack{\sigma\{\mathrm{d}\}\neq 0,\\ \sigma\{\sigma_e\}=0}}\ \sigma\{I\}\big|_{\substack{\sigma\{\mathrm{d}\}=0,\\ \sigma\{\sigma_e\}\neq 0}}\ \rho\{\mathrm{d},\sigma_e\}\end{array}} \tag{15}$$

In our case, it has been considered that both parameters are independent (non-correlated) $\rho\{\mathrm{d},\sigma_e\} = 0$, and $\sigma\{I_{\mathrm{w}}\}$ of the

[2]This CPU time was achieved thanks to a permittivity scaling algorithm to accelerate the low-frequency convergence [16], starting from an initial time step of 10 ps, to achieve in 10^6 time steps a total physical time of 24 μs.

combined distribution is obtained as the square root of the addition of the square of each separate $\sigma\{\}$,

$$\sigma\{I_{\mathrm{w}}\} = \sqrt{\sigma^2\{I\}\big|_{\substack{\sigma\{\mathrm{d}\}\neq 0,\\ \sigma\{\sigma_e\}=0}} + \sigma^2\{I\}\big|_{\substack{\sigma\{\mathrm{d}\}=0,\\ \sigma\{\sigma_e\}\neq 0}}} \quad (16)$$

(see [8] for a discussion on this).

As a guess, we can employ an equivalent circuit model to corroborate the findings obtained from MC-FDTD and S-FDTD methods, given that the LIE test case operates at a very low frequency. This model consists of three resistances (Fig. 5): R_s and R_p are the series and parallel resistances, respectively, from the perspective of the thin wire. R_w represents the resistance of the thin wire, which is the sum of the two loads at its ends, equal to 100Ω. The resistance R_p can be expressed analytically in terms of d and σ, and it takes the following form:

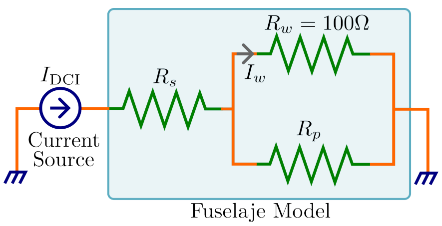

Fig. 5. Low-frequency circuit model of the fuselage.

$$R_p(\sigma_e, \mathrm{d}) = \frac{1}{\sigma_e\,(A\,\mathrm{d} + B)} \quad (17)$$

where A and B are geometrical factors determined heuristically, yielding in our case values of $A = 1.258$ and $B = 1.794 \cdot 10^{-5}$ respectively. Finally, we can determine the current passing through the thin wire, denoted as I_{w}, as a function of the injected current I_{DCI},

$$\begin{aligned} I_w(\sigma_e, \mathrm{d}) &= I_{\mathrm{DCI}}\frac{R_p(\sigma_e, \mathrm{d})}{R_p(\sigma_e, \mathrm{d}) + R_w} = \\ &= I_{\mathrm{DCI}}\frac{1}{1 + 100\,\sigma_e\,(A\,\mathrm{d} + B)} \end{aligned} \quad (18)$$

The results in the time domain of the mean and standard deviation of I_w obtained with MC-FDTD, S-FDTD, and the circuit model are cross-compared in Fig. 6, for the MC method (MC-FDTD and MC-Circuit) we used 20,000 iterations. Fig.7 shows the PDF normalized of the I_{w} normalized in time to I_{DCI}, as a reference, we include the PDF for the MC-circuit with 10^7 iterations. It should be noted that the S-FDTD method does not involve any PDF. For the results in Fig.7, we have assumed that it follows a Gaussian propagation, and the validity of this assumption depends on how good the approximation (14) is. Finally, the table II shows a comparison of the mean and standard deviation of the PDFs.

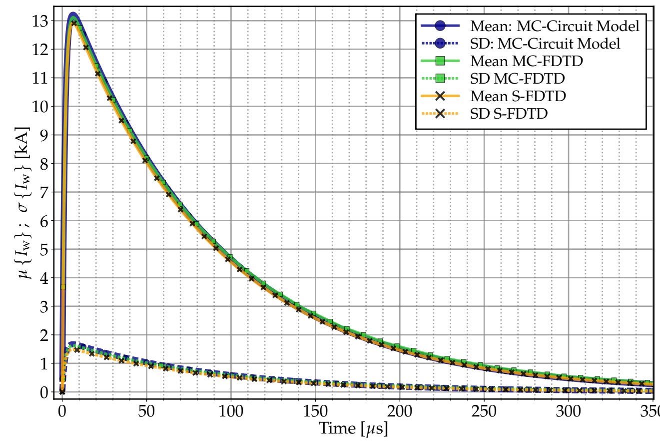

Fig. 6. Comparison of current coupled to the wire considering CFC conductivity and thickness as uncorrelated variables.

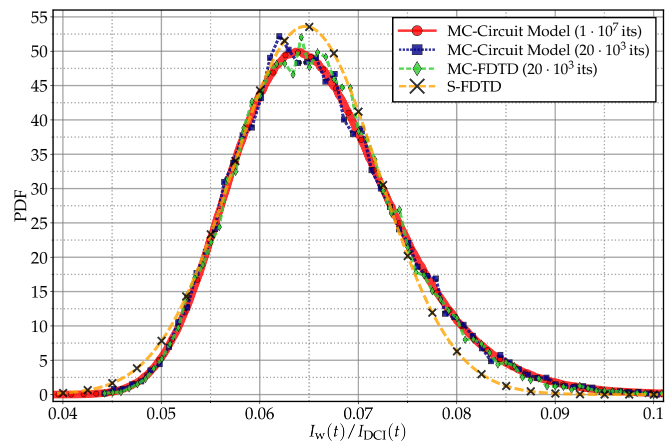

Fig. 7. Comparison of current coupled to the wire considering CFC conductivity and thickness as uncorrelated variables.

TABLE II
MEAN AND STANDARD DEVIATION RESULTS OF THE CURRENT IN THE WIRE FOR A GAUSSIAN PDF.

$\mu\{I_{\mathrm{w}}(1)/I_{\mathrm{DCI}}(t)\}$; $\sigma\{I_{\mathrm{w}}(1)/I_{\mathrm{DCI}}(t)\}$			
MC-Circuit 10^7 its	MC-Circuit $20 \cdot 10^3$ its	MC-FDTD $20 \cdot 10^3$ its	S-FDTD
0.0661; 0.0841	0.0660; 0.0083	0.066; 0.0081	0.0646; 0.0074

VI. CONCLUSIONS

In this work, we employ the classical S-FDTD explicit algorithm and extend it to an HIE algorithm. Specifically, we present a method for analyzing thin panel structures using the S-FDTD method in conjunction with the CN-SGBC subcell method. A simple methodology to build stochastic versions of other FDTD or HIE-FDTD methods can be inferred from the approach described in this paper, indicating how to implement them into existing codes. The implementation of the S-FDTD for thin wires of [8] are also prone to be combined with the CN-SGBC one for thin panels shown in this paper to find the currents induced at each end of the wire, including the wire radii and loads uncertainties.

Validations for a simple thin panel with uncertainties in its thickness, using MC analysis, have been presented. Finally, we have also shown that the presented method allows us to estimate correctly the stochastic behavior of the induced currents in wires due to LIE on composite aircraft, employing a simple yet representative example of an aeronautical situation. The presented method also demonstrates no additional constraints to the usual stability criterion.

The provided PDF results show comprehensive statistical information on the uncertainties obtained in the electromagnetic magnitudes. Similar to other extensions of the S-FDTD method, bearing in mind that the accuracy of the mean and standard deviation determined by the S-FDTD method, can only be interpreted within a linear regime when the standard deviation of the input parameters is small.

References

[1] K. Yee, "Numerical solution of initial boundary value problems involving Maxwell's equations in isotropic media," *IEEE Transactions on Antennas and Propagation*, vol. 14, no. 3, pp. 302–307, May 1966.

[2] A. Taflove and S. C. Hagness, *Computational Electrodynamics The Finite-Differences Time Domain Method*. Artech House, 2005.

[3] M. Sarto, "A new model for the FDTD analysis of the shielding performances of thin composite structures," *Electromagnetic Compatibility, IEEE Transactions on*, vol. 41, no. 4, pp. 298 –306, Nov. 1999.

[4] I. D. Flintoft, S. A. Bourke, J. F. Dawson, J. Alvarez, M. R. Cabello, M. P. Robinson, and S. G. Garcia, "Face-centered anisotropic surface impedance boundary conditions in FDTD," *IEEE Transactions on Microwave Theory and Techniques*, vol. 66, no. 2, pp. 643–650, Feb. 2018.

[5] M. Ruiz Cabello, L. Diaz Angulo, J. Alvarez, I. D. Flintoft, S. Bourke, J. F. Dawson, R. Gómez Martín, and S. G. Garcia, "A hybrid crank–nicolson fdtd subgridding boundary condition for lossy thin-layer modeling," *IEEE Transactions on Microwave Theory and Techniques*, vol. 65, no. 5, pp. 1397–1406, 2017.

[6] J. Zhong, B. Feng, L. Yan, X. Zhao, Q. Liu, X. Meng, and H. Zhou, "Fdtd-based shielding effectiveness prediction of enclosures made of composite materials," in *2020 IEEE MTT-S International Conference on Numerical Electromagnetic and Multiphysics Modeling and Optimization (NEMO)*. IEEE, 2020, pp. 1–4.

[7] S. M. Smith and C. Furse, "Stochastic fdtd for analysis of statistical variation in electromagnetic fields," *IEEE Transactions on Antennas and Propagation*, vol. 60, no. 7, pp. 3343–3350, July 2012.

[8] S. G. Garcia, M. R. Cabello, L. D. Angulo, A. R. Bretones, M. G. Atienza, and E. Pascual-Gil, "Application of stochastic FDTD to holland's thin-wire method," *IEEE Antennas and Wireless Propagation Letters*, vol. 18, no. 10, pp. 2046–2050, Oct. 2019.

[9] R. Holland and L. Simpson, "Finite-difference analysis of EMP coupling to thin struts and wires," *Electromagnetic Compatibility, IEEE Transactions on*, vol. EMC-23, no. 2, pp. 88 –97, may 1981.

[10] K. Masumnia-Bisheh, K. Forooraghi, M. Ghaffari-Miab, and C. M. Furse, "Geometrically stochastic fdtd method for uncertainty quantification of em fields and sar in biological tissues," *IEEE Transactions on Antennas and Propagation*, vol. 67, no. 12, pp. 7466–7475, 2019.

[11] C. Salis, N. Kantartzis, and T. Zygiridis, "A stochastic finite-difference time-domain (fdtd) method for assessing material and geometric uncertainties in rectangular objects," *Technologies*, vol. 8, no. 1, p. 12, 2020.

[12] M. R. Cabello, L. Diaz Angulo, A. R. Bretones, M. Fernandez Pantoja, and S. G. Garcia, "Application of stochastic FDTD to thin-wire analysis," in *Proc. Int. Symp. Electromagnetic Compatibility - EMC EUROPE*, Sep. 2019, pp. 917–920.

[13] K. M. Bisheh, B. Z. Gatabi, and S. M. H. Andargoli, "Stochastic fdtd accuracy improvement through correlation coefficient estimation," *Waves in Random and Complex Media*, vol. 25, no. 2, pp. 154–169, 2015. [Online]. Available: https://doi.org/10.1080/17455030.2014.999845

[14] G. A. Rasek, E. Pascual-Gil, A. Schröder, I. Junqua, R. Guidi, C. A. Kreller, H.-D. Brüns, and S. E. Loos, "Hirf transfer functions of a fuselage model: Measurements and simulations," *IEEE Transactions on Electromagnetic Compatibility*, vol. 56, no. 2, pp. 311–319, 2014.

[15] *Aircraft Lightning Test Methods, EUROCAE ED-105, rev A*, EUROCAE ED-107A /SAE ARP5583A Std., 2013.

[16] Yik-Kiong Hue, F. L. Teixeira, L. S. Martin, and M. S. Bittar, "Three-dimensional simulation of eccentric lwd tool response in boreholes through dipping formations," *IEEE Transactions on Geoscience and Remote Sensing*, vol. 43, no. 2, pp. 257–268, 2005.